NeuroImage: Clinical 37 (2023) 103306

Contents lists available at ScienceDirect

NeuroImage: Clinical

journal homepage: www.elsevier.com/locate/ynicl

Gray matter microstructure differences in autistic males: A gray matter based spatial statistics study

Marissa A. DiPiero [a,b], Olivia J. Surgent [a,b], Brittany G. Travers [a,d,e], Andrew L. Alexander [a,c,f], Janet E. Lainhart [a,c], Douglas C. Dean III [a,f,g,*]

[a] Waisman Center, University of Wisconsin–Madison, Madison, WI, USA
[b] Neuroscience Training Program, University of Wisconsin–Madison, Madison, WI, USA
[c] Department of Psychiatry, University of Wisconsin School of Medicine and Public Health, Madison, WI, USA
[d] Occupational Therapy Program, University of Wisconsin–Madison, Madison, WI, USA
[e] Department of Kinesiology, University of Wisconsin–Madison, Madison, WI, USA
[f] Department of Medical Physics, University of Wisconsin–Madison, Madison, WI, USA
[g] Department of Pediatrics, University of Wisconsin–Madison, Madison, WI, USA

ARTICLE INFO

Keywords:
GBSS
Gray matter microstructure
Autism
NODDI
DTI
Childhood
Adolescence

ABSTRACT

Background: Autism spectrum disorder (ASD) is a complex neurodevelopmental condition. Understanding the brain's microstructure and its relationship to clinical characteristics is important to advance our understanding of the neural supports underlying ASD. In the current work, we implemented Gray-Matter Based Spatial Statistics (GBSS) to examine and characterize cortical microstructure and assess differences between typically developing (TD) and autistic males.

Methods: A multi-shell diffusion MRI (dMRI) protocol was acquired from 83 TD and 70 autistic males (5-to-21-years) and fit to the DTI and NODDI models. GBSS was performed for voxelwise analysis of cortical gray matter (GM). General linear models were used to investigate group differences, while age-by-group interactions assessed age-related differences between groups. Within the ASD group, relationships between cortical microstructure and measures of autistic symptoms were investigated.

Results: All dMRI measures were significantly associated with age across the GM skeleton. Group differences and age-by-group interactions are reported. Group-wise increases in neurite density in autistic individuals were observed across frontal, temporal, and occipital regions of the right hemisphere. Significant age-by-group interactions of neurite density were observed within the middle frontal gyrus, precentral gyrus, and frontal pole. Negative relationships between neurite dispersion and the ADOS-2 Calibrated Severity Scores (CSS) were observed within the ASD group.

Discussion: Findings demonstrate group and age-related differences between groups in neurite density in ASD across right-hemisphere brain regions supporting cognitive processes. Results provide evidence of altered neurodevelopmental processes affecting GM microstructure in autistic males with implications for the role of cortical microstructure in the level of autistic symptoms.

Conclusion: Using dMRI and GBSS, our findings provide new insights into group and age-related differences of the GM microstructure in autistic males. Defining where and when these cortical GM differences arise will contribute to our understanding of brain-behavior relationships of ASD and may aid in the development and monitoring of targeted and individualized interventions.

1. Introduction

Autism spectrum disorder (ASD) is a complex, heterogeneous neurodevelopmental condition believed to arise from deviations during brain development. Amid the increasing evidence that implicates a diverse range widespread brain alterations associated with ASD (Prigge et al., 2021; Edgar et al., 2019; Uono et al., 2022; Lange et al., 2015; Travers et al., 2015; Green et al., 2022; Dean et al., 2016; Surgent et al.,

* Corresponding author at: Waisman Center, University of Wisconsin–Madison, Madison, WI 53705, USA.
E-mail address: deaniii@wisc.edu (D.C. Dean III).

https://doi.org/10.1016/j.nicl.2022.103306
Received 6 October 2022; Received in revised form 29 November 2022; Accepted 24 December 2022
Available online 26 December 2022

2021), differences within the cerebral cortex appear to play an important role. Studies of post-mortem brain tissue have reported an array of cellular differences in the cortex of autistic individuals in neuronal size, number, and density (Courchesne et al., 2011), irregular laminar patterns (Amaral et al., 2008); glial cell abnormalities (Vargas et al., 2005), and decreased size and density of dendritic arbors (Palmen et al., 2004). In-vivo studies utilizing magnetic resonance imaging (MRI) have highlighted differential patterns of cortical morphology in ASD compared to non-autistic individuals, including differences in cortical volumes (Hazlett et al., 2005, 2011; Lainhart, 2015; Mensen et al., 2017; Minshew and Williams, 2007), thickness (Hazlett et al., 2011; Mensen et al., 2017; Smith et al., 2016; Wallace et al., 2015; Zielinski et al., 2014; Hardan et al., 2009; Khundrakpam et al., 2017), surface area (Hazlett et al., 2011; Smith et al., 2016; Ohta et al., 2016; Ecker et al., 2013; Piven et al., 2017) and gyrification (Wallace et al., 2015; Kohli et al., 2019; Williams et al., 2012; Hardan et al., 2004; Yang et al., 2016), regional variations of atypical brain overgrowth in early childhood (Courchesne et al., 2001, 2003, 2011; Hazlett et al., 2005; Nordahl et al., 2011), and diverging longitudinal age-related trajectories (Prigge et al., 2021; Lange et al., 2015; Hardan et al., 2009; Nunes et al., 2020) in autistic individuals. Together, these postmortem and neuroimaging findings implicate gray matter (GM) morphology and cytoarchitecture in the biological basis of ASD; however, the architecture and organization of the cortical microstructure has not been extensively investigated.

Diffusion MRI (dMRI) probes the neural microstructure by characterizing the random motion of water molecules in tissue (Afzali et al., 2021; Basser and Ozarslan, 2009). Alterations in the density and/or organization of the diffusion barriers imposed by components of tissue microstructure can restrict water diffusion. Diffusion tensor imaging (DTI) is the most widely used dMRI technique to study the brain's microstructure and enables quantitative estimation of four scalar indices: fractional anisotropy (FA), and mean (MD), radial (RD), and axial (AD) diffusivity. DTI metrics have been widely used to study the white matter microstructure across the lifespan and in neurodevelopmental disorders, including ASD (for review see refs: Travers et al. (2015); Ameis and Catani (2015)). However, studies utilizing DTI to assess cortical GM microstructure have been limited. Widespread reductions in GM FA and increased MD in autistic compared to typically developing (TD) individuals have been reported (Bletsch et al., 2021). Similar reports of FA reductions Pichiecchio and Carigi, (2016) and MD increases (Bletsch et al., 2021; Groen et al., 2011) in ASD suggest cortical microstructural differences to be associated with ASD. However, several limitations of the DTI model make it challenging to analyze and interpret DTI metrics in GM, including the assumption of a Gaussian diffusion distribution within complex microstructure of the cortical GM (Wheeler-Kingshott and Cercignani, 2009) and bias from partial volume effects of the CSF (Alexander et al., 2001).

Recent advancements in dMRI acquisition and modeling have aimed to address several limitations of DTI and improve the characterization of the neural microstructure (Alexander et al., 2019). Specifically, multi-shell dMRI methods are used to account for more complex diffusion signal changes, including changes resulting from non-Gaussian diffusion distributions or multiple compartments of diffusion (Alexander et al., 2019), making such methods especially applicable to investigations of the cortical microstructure. Neurite orientation dispersion and density imaging (NODDI) (Zhang et al., 2012) is one multi-compartment biophysical model that quantifies the angular variation of neurites with orientation dispersion index (ODI) and intracellular volume fraction of neurites (FICVF). NODDI also accounts for a wide range of neurite orientation distributions that capture the full spectrum of patterns observed across brain tissue, including the highly disperse dendritic processes of the cortical GM microstructure (Zhang et al., 2012).

Still, few studies have utilized dMRI to examine the GM microstructure in ASD. For example, one study observed their ASD group to have significantly increased MD across several GM regions compared to controls (Groen et al., 2011). Using Restricted Spectrum Imaging (RSI), an alternative multi-shell, multicompartment dMRI technique, Carper et al. observed decreased neurite density and increased MD in ASD compared to TDs, though only a localized neurite density decrease in the left temporal occipital fusiform gyrus survived multiple comparison correction (Carper et al., 2016). A recent diffusion kurtosis imaging (DKI) study described decreased mean kurtosis (MK) and radial kurtosis (RK) and MD in young autistic males compared to TD males, in frontal, parietal and temporal cortical regions (McKenna et al., 2020). In the same study, this decreased GM MK was associated with increased repetitive and restricted behaviors and impaired social interaction (McKenna et al., 2020). Further, a study utilizing NODDI in GM report increased ODI in visual brain areas of autistic adults that was related to altered visual processing (Matsuoka et al., 2020). Decreased NODDI neurite density and ODI were also observed in regions of the ventral occipital complex, fusiform gyrus, inferior parietal and superior temporal regions in ASD with impaired recognition of facial emotional expressions (Yasuno et al., 2020), while significantly increased NODDI ODI of the left occipital gyrus has additionally been observed in adults with ASD (Matsuoka et al., 2020). While these findings provide *in vivo* evidence of differential GM microstructure in ASD and demonstrates the utility of dMRI methods to detect cortical differences, a dearth of studies have explicitly investigated age-related differences in GM microstructure in ASD.

The current study utilizes multi-shell dMRI to investigate cortical microstructural differences between autistic and non-autistic children and young adults. We applied the Gray Matter Based Spatial Statistics (GBSS) framework (Nazeri et al., 2017), which utilizes NODDI measures to reduce partial volume contamination and improve sensitivity of dMRI measures in GM, to assess cortical GM differences in autistic males. Cross-sectional age-related group differences were additionally assessed to investigate whether cortical maturation patterns may differ between groups. We hypothesized the ASD group to demonstrate wide-spread cortical differences compared to the TD group, namely decreased neurite density and increased dispersion. Given the reports of brain overgrowth from infancy to childhood (Courchesne et al., 2001, 2003, 2011; Hazlett et al., 2005; Nordahl et al., 2011), we hypothesize faster age-related changes in cortical maturation in ASD in our sample. Further, we examined associations between cortical GM and the ADOS-2 Calibrated Severity Score (CSS), a reliable measure of level of autistic symptoms (Hus and Lord, 2014), and the Social Responsiveness Scale (SRS), which identifies the presence and severity of social impairment in ASD (Constantino and Gruber, 2012). Given previous findings in ASD between cortical thickness and CSS (Bedford et al., 2020) and SRS (Prigge et al., 2018), we hypothesized that cortical microstructure measures in ASD to be associated with these clinical scores such that individuals with higher ASD severity would demonstrate lower neurite density, representing thinner axonal and dendritic arborizations, in brain areas supporting social behaviors. To our knowledge, the current study is the first to utilize GBSS to characterize cortical GM microstructure in ASD and to investigate NODDI metrics as a potential marker of differential cortical microstructure related to ASD.

2. Materials and methods

2.1. Participants

Participants in this cross-sectional study were pooled from two neuroimaging studies at the University of Wisconsin–Madison investigating patterns of brain microstructure in ASD. Across these studies, a total of 70 ASD and 83 TD males between 5.8 and 21.75 years of age were included. For specific inclusion/exclusion criteria see **Supplemental Text**.

All participants were able to communicate verbally and had a nonverbal IQ score > 60, as measured by the Wechsler Abbreviated Scale of Intelligence, 2nd Edition (WASI-II; (Da, 2011)). Participants in the ASD group had a previous clinical diagnosis of ASD and were

confirmed to meet DSM 5 criteria for ASD (Association et al., 2013) upon enrollment, based on all information available including assessment with standardized measures (see **Supplemental Text**). ASD and TD subjects did not differ on age ($p = 0.390$), while ASD participants were observed to have a significantly lower full-scale IQ ($p = 0.0002$). Participant demographic information can be found in Table 1. 54 % (38/70) of the ASD subjects were prescribed a psychotropic medication, including stimulants, anti-psychotics, and serotonin reuptake inhibitors (SSRIs).

3. Imaging acquisition and processing

Imaging data were acquired at the Waisman Center at the University of Wisconsin-Madison on the same 3.0 Tesla GE Discovery MR750 scanner (Waukesha, WI) equipped with a 32-channel phase array head coil (Nova Medical, Wilmington, MA). Diffusion weighted images (DWIs) were acquired using a multi-shell spin-echo echo-planar pulse sequence for both participant cohorts. A total of 69 DWIs were acquired, 6 of which were acquired with no diffusion encoding (i.e., b-value = 0 s/mm^2) and the remaining 63 images acquired along non-collinear diffusing encoding directions with b = 350 s/mm^2 [9 directions], b = 800 s/mm^2 [18 directions], and b = 2000 s/mm^2 [36 directions]. Additional image acquisition parameters were moderately different between the two participant cohorts. For one cohort, images were acquired with a field of view of 230 mm × 230 mm and in-plane resolution of 2.4 mm × 2.4 mm, interpolated with zero-filling to 1.8 mm × 1.8 mm; 76 slices with a slice thickness 3.6 mm and slice spacing −1.8 mm; repetition time (TR) = 9000 ms; and echo time (TE) = 74.4 ms. Scanning parameters for the second cohort consisted of a 256 mm × 256 mm field of view and in-plane resolution of 2.0 mm × 2.0 mm; 70 slices with a slice thickness of 2 mm; TR = 8575 ms; and TE = 76.9 ms. For both acquisitions, the approximate duration of the dMRI scan was 10 min.

Following image acquisition, DWIs were processed using inhouse processing pipelines. Briefly, DWIs underwent Rician noise (Veraart et al., 2016) and Gibbs ringing artifact correction (Kellner et al., 2016) using MRtrix3 (Tournier et al., 2019). The FMRIB software library (FSL; (Jenkinson et al., 2012)) *eddy* tool was used to correct for motion and eddy current-induced distortions (Andersson and Sotiropoulos, 2016), while outlier detection and replacement was enabled to identify and correct for signal dropout artifacts (Andersson et al., 2016). Gradient directions were corrected for rotations (Leemans and Jones, 2009) and non-parenchyma signal was removed (Smith, 2002). Diffusion tensors were estimated at each voxel using a weighted-least squares algorithm as part of the diffusion imaging in python (DIPY) open-source software package (Garyfallidis et al., 2014). Quantitative maps of fractional anisotropy, and mean, radial and axial diffusivity (FA, MD, RD, AD, respectively) were derived (Basser, 1995). DWIs were also fit to the three-compartment NODDI tissue model (Zhang et al., 2012) in Python using Accelerated Microstructure Imaging via Convex Optimization (AMICO) (Daducci et al., 2015), to provide estimates of the intracellular volume fraction (density) of neurites (FICVF), orientation dispersion index (ODI) and isotropic volume fractions (FISO). Quantitative maps were visually inspected for artifacts (i.e. slice intensity banding, FA hyper-intensities, distortions, and/or blurring). To account for acquisition protocol differences between the two study cohorts, DTI (FA, MD, RD, AD) and NODDI (FICVF, ODI, FISO) parameter maps were harmonized using the NeuroHarmonize software package (Pomponio et al., 2020). NeuroHarmonize, an extension of the ComBat framework (Fortin et al., 2018), uses an empirical Bayes approach, while preserving variability in across additional covariates of interest (e.g. age).

Table 1
Demographic, cognitive, and clinical characteristics of participants.

Sample Demographics	TD	ASD	*p value*
N	83	70	–
Age (Years); Mean (SD) [Range]	12.72 (4.70) [5.75 – 21.75]	12.11 (3.82) [6.4 – 21.0]	p = 0.390
Race			
Black	1	1	–
Asian	0	2	–
White	76	62	–
Multi-Racial	5	3	–
Not Reported/missing	1	2	–
Clinical Characteristics average score (SD) [Range]			
ADOS-2 CSS	–	7.11 (2.16)	–
SRS Total T Score	–	76.38 (10.73)	–
Full Scale IQ	113.46 (12.41) [83 – 139]	104.04 (18.71) [63–140]	p = 0.0002*

** ADOS- CSS scores collected in n = 59 ASD participants; SRS scores collected in n = 65 ASD participants; Full-scale IQ collected in n = 87 TD n = 69 ASD. * indicates significance.

4. GM-based spatial statistics (GBSS)

GBSS adopts the tract-based spatial statistics (TBSS) (Smith et al., 2006) framework to allow for analysis of diffusion MRI measures in the cortical GM (Nazeri et al., 2015, 2017). Processing steps for GBSS have been previously described (Nazeri et al., 2015, 2017). Briefly, a two-tissue class segmentation of the DTI FA maps was performed using *Atropos* (Avants et al., 2011) to estimate a white matter fraction map. GM fraction maps were then estimated by subtracting the white matter fraction and CSF fraction (NODDI FISO parameter) maps from 1. Tissue class segmentation maps were multiplied by their corresponding tissue weighting (0 = CSF, 1 = GM, and 2 = white matter) and summed together to generate a 'pseudo T1-weighted' image (Nazeri et al., 2017). Pseudo T1-weighted images from each subject were used to build a study-specific template using the *buildtemplateparallel.sh* script as part of the Advanced Normalization Tools (ANTs) software suite (Avants et al., 2008, 2010). DTI and NODDI measures and GM fraction maps were non-linearly warped into the study-specific template space by applying the warp fields generated by template construction. GM fraction maps aligned to the study-specific template were averaged to create a mean GM fraction map, which was skeletonized using the *tbss_skeleton* tool in FSL (Fig. 1; (Jenkinson et al., 2012; Smith et al., 2006). NODDI and DTI metrics were projected onto the GM skeleton from local voxels with the greatest GM fraction. The GM skeleton was thresholded to include only voxels with an average GM fraction > 0.65 (Nazeri et al., 2017).

5. Statistical analyses

5.1. Cortical microstructural age associations

Given the cortex is undergoing rapid growth across the lifespan (Fan and Jiang, 2017; Gogtay et al., 2004; Lebel et al., 2008; Tamnes et al., 2010; Turesky et al., 2021), we first assessed age-related associations across the GM skeleton. For each subject, average values of FICVF, ODI, FA, MD, RD, and AD were extracted from the GM skeleton and used to construct an overall cortical microstructure trajectory. Without accounting for group membership, candidate linear (dMRI(age) ~ α*age + β) and logarithmic (dMRI(age) ~ α*ln(age) + β) growth models were fit to the cortical microstructure measures on a voxelwise basis using RStudio (Version 2021.09.2 + 382 "Ghost Orchid") (R Core Team, 2021). Significance was defined as $p < 0.05$, corrected for false discovery rate. Information criterion parameters, including the Bayesian Information Criterion (BIC) and Akaike information criterion (AIC), were calculated and used to evaluate the model that best fit the data. The best fitting model for each dMRI parameter was subsequently used to investigate population-wise age relationships and differential cortical microstructural patterns between groups. See **Supplemental Text** for more information about candidate model selection.

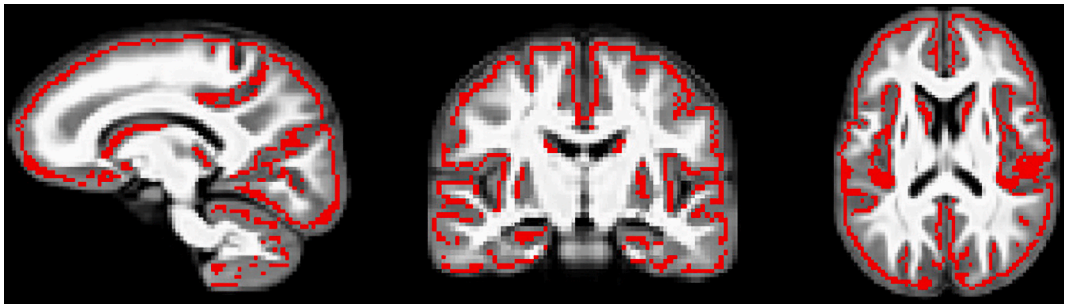

Fig. 1. GBSS GM skeleton projected on study-specific template. GM fraction maps were first averaged across subjects and the mean GM image was skeletonized (red). All DTI and NODDI metrics and GM fraction were projected onto the skeleton from the local GM fraction maxima. (For interpretation of the references to colour in this figure legend, the reader is referred to the web version of this article.)

5.2. ASD and TD group differences in cortical microstructure

General Linear Models (GLMs) were used to investigate cortical microstructural differences between groups, while age-by-group interactions were used to investigate potential age-related group differences. Group difference and age-by-group interaction models were run separately. Based on the outcome of our BIC and AIC for model fitting described above, logarithmic age was controlled for in the group difference models for measures of FICVF, FA, MD, RD, and AD, while linear age was controlled for in the GLMs of ODI (Table 2**)**. Covariates in all analyses were centered. Non-parametric permutation testing with tail approximation (n = 500) was carried out using Permutation Analysis of Linear Models (PALM) (Smith et al., 2006; Winkler et al., 2014). We applied the tail approximation method in PALM as recommended by Winkler et al. (2016) for methods including familywise error correction of p-values to utilize a smaller number of permutations by fitting the tail of the permutation distribution to the fit of a generalized Pareto distribution (GPD) (James, 1975; Winkler et al., 2016), from which the p-values are computed. A multivariate analysis was used for GM DWI measures following a logarithmic age pattern. A univariate analysis was run separately for ODI. Joint inference of group differences was assessed with the non-parametric combination (NPC) and Fisher's combining function across five dMRI metrics: FICVF, FA, MD, AD and RD, while differences in individual metrics were also evaluated. Threshold free cluster enhancement (TFCE) (Smith and Nichols, 2009) was used to identify significant regions at $p < 0.05$, FWER-corrected across modality and contrast. Overlapping voxels displaying a significant group and age-by-group interaction were removed from group difference findings for ease of interpretation.

5.3. Associations with ADOS-2 CSS and SRS

Level of autistic symptoms observed by researchers at study enrollment was quantified with the ADOS-2 (Lord et al., 2000). To allow comparison of ADOS total scores across ages and modules, the calibrated severity score (CSS) was used. CSS is considered a reliable measure of the level of autistic symptoms (Hus and Lord, 2014) and ranges from 1-to-10 (with 10 being the most severe) (Gotham et al., 2009). Considering the ASD group only, non-parametric inference of voxelwise GBSS-skeletonized DTI and NODDI measures were estimated by linear regression using PALM and n = 500 permutations, controlling for the effects of age and IQ. Significance was defined as $p < 0.05$, FWER-corrected using TFCE (Smith et al., 2006). Associations between CSS and GM microstructure were run separately excluding IQ as a covariate. Correlations of SRS, ADOS-CSS, and IQ can be found in **Supplement Table 5.**

A similar approach was used to investigate associations between cortical microstructural metrics and a standardized questionnaire completed by parents, the Social Responsiveness Scale (SRS;(Constantino and Gruber, 2012). The SRS was developed as a quantitative scale that measures the presence and extent of autistic social impairment. The SRS total *T*-score was used in analysis. Non-parametric inference of voxelwise GBSS-skeletonized DTI and NODDI measures were estimated by linear regression using PALM with n = 500 permutations controlling for the effects of age and IQ. Significance was defined as $p < 0.05$, FWER-corrected using TFCE (Smith et al., 2006) controlling for the effects of age and IQ. Additional analyses were conducted excluding IQ as a covariate.

To identify significant brain regions, statistical maps were linearly co-registered to the Harvard-Oxford Cortical atlas (Desikan et al., 2006; Frazier et al., 2005; Goldstein et al., 2007; Makris et al., 2006; Jenkinson et al., 2002) using FSL's flirt tool.

6. Results

6.1. Cortical microstructural age associations

Logarithmic growth models were found to best describe the age-related trajectories for FICVF, FA, MD, AD, and RD, while the linear model was more appropriate for ODI. BIC and AIC values from comparison of logarithmic and linear age models are provided in Table 2**.** Average age-related patterns of GBSS-skeletonized diffusion MRI metrics are shown in Fig. 2. In general, FA, FICVF and ODI are observed to increase with age, while MD, RD, and AD decreased with age.

To further assess the cortical microstructural age relationships, GBSS-skeletonized DTI and NODDI measures were fit to logarithmic and linear growth models to assess voxelwise age-related changes. Across the GBSS skeleton, age-related patterns were generally consistent with the mean age-related trajectories for each measure described in Fig. 2. Measures of FA, FICVF, and ODI tended to increase with age ($p < 0.05$; FWER-corrected) across the GBSS skeleton, while measures of MD, RD, and AD tended to decrease with age ($p < 0.05$; FWER-corrected).

Table 2
BIC & AIC age fitting: selection of best fit for linear and logarithmic age.

	FICVF	ODI	FA	MD	RD	AD
BIC: Log Age	**−989.07**	−920.87	**−1136.79**	**−2954.10**	**−2968.55**	**−2916.34**
BIC: Linear Age	−978.11	**−929.08**	−1135.24	−2948.64	−2961.84	−2913.61
AIC: Log Age	**−998.16**	−911.79	**−1145.88**	**−2963.20**	**−2977.64**	**−2925.43**
AIC: Linear Age	−987.20	**−919.99**	−1144.33	−2957.73	−2970.93	−2922.71

** bolded values indicate best fit.

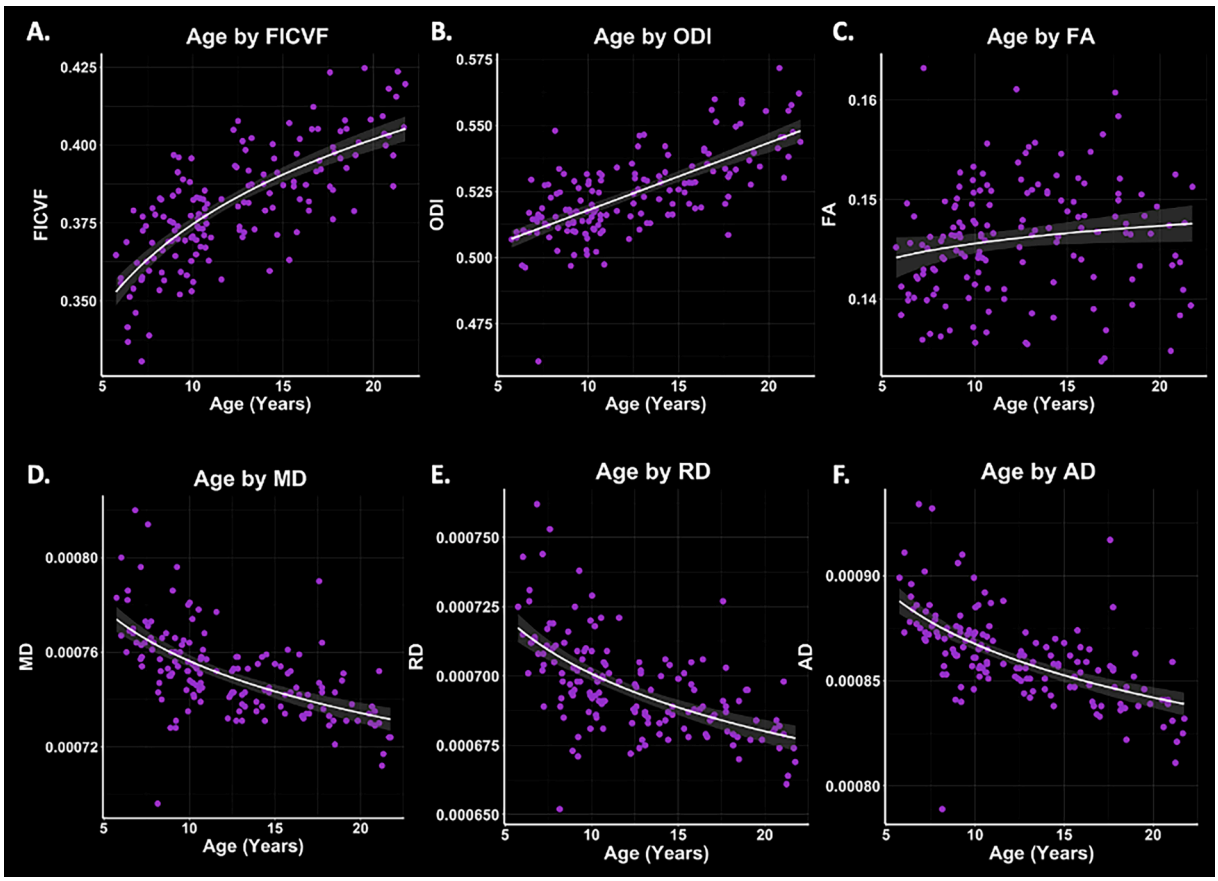

Fig. 2. Cortical GM microstructure age relationships. Logarithmic and linear fit lines applied per BIC and AIC model selection in Table 2. Scatter points represent mean dMRI measures across the GM skeleton shown in Fig. 1. Bands represent confidence intervals.

Statistical maps for significant age relationships can be visualized in Fig. 3.

6.2. ASD and TD group differences in cortical microstructure

Voxelwise GBSS group comparisons revealed significant ($p < 0.05$, FWER-corrected) FICVF, MD, RD, and AD differences between ASD and

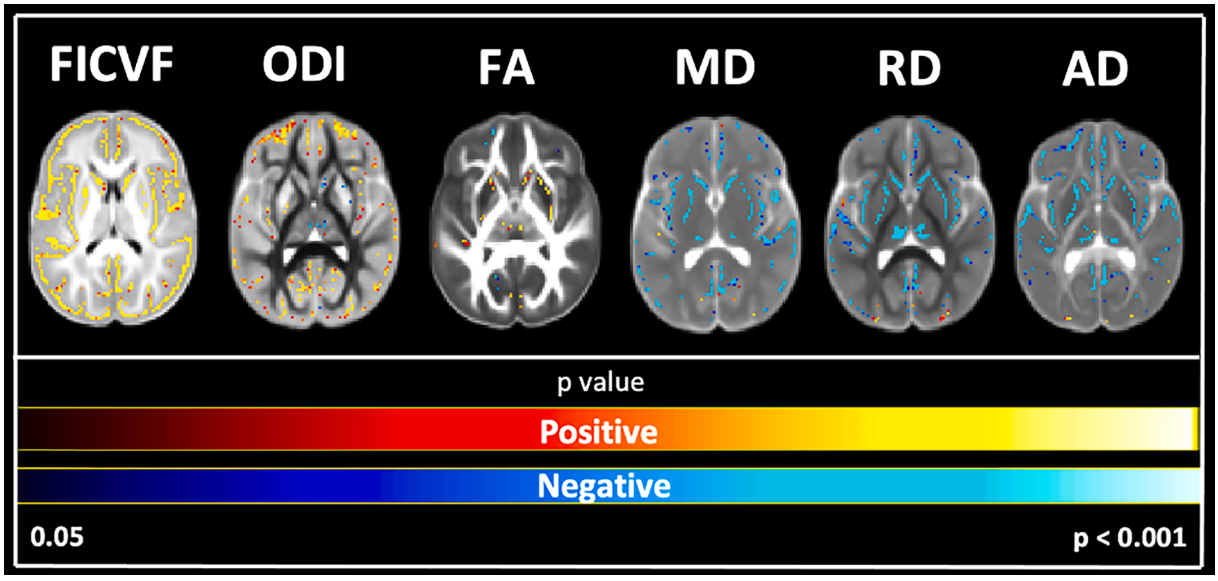

Fig. 3. Voxel-based age relationships of cortical GM microstructure. Logarithmic and linear fits applied per BIC and AIC model selection in Table 2. Significant positive (Yellow/Red) and negative (Light blue/Dark Blue) voxels are shown on the dMRI maps for each measure. Voxels showing significant negative relationships are shown in blue while voxels showing significant positive relationships are shown in red. (For interpretation of the references to colour in this figure legend, the reader is referred to the web version of this article.)

TD groups (Fig. 4). The ASD group demonstrated lower FICVF, and higher MD, RD, and AD compared to the TD group across frontal and temporal brain regions concentrated in the right hemisphere. FICVF, MD, RD, and AD were all observed to differ between the groups in the right frontal pole. Group differences of FICVF were observed across frontal, temporal, and occipital regions of the right hemisphere (Fig. 4**A, Supplement** Table 1). Group differences of MD were found in right hemisphere frontal brain regions, whereas RD group differences were observed in right hemisphere frontal and insular cortices, and AD group differences spanned frontal, temporal, and parietal lobes of the right hemisphere (Fig. 4**B — 4D).** No significant group differences were observed for measures of FA and ODI. All neuroanatomical locations of

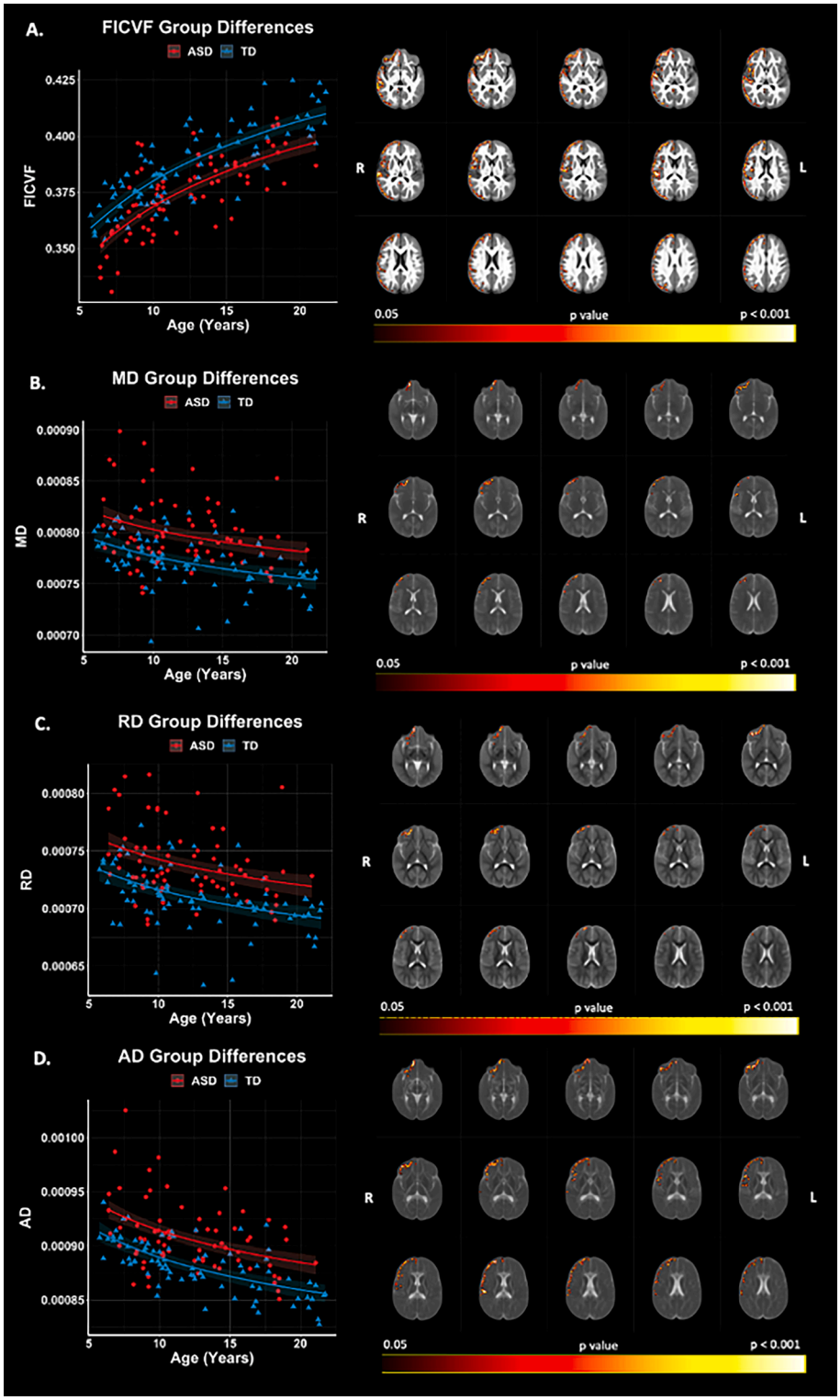

Fig. 4. Group differences in NODDI and DTI measures. Level of significance and neuroanatomical location of voxels from group difference model are displayed on the mean dMRI maps from all participants. Scatter points represent mean dMRI values of significant voxels for each measure. Trendlines show model fit and confidence intervals for group difference on dMRI measures when accounting for age.

significant group differences by dMRI measure can be found in **Supplement** Table 1**.**

6.3. Age-by-Group interactions in cortical microstructure

GBSS voxelwise analysis showed significant ($p < 0.05$, FWER-corrected) age-by-group interactions on FICVF in the right hemisphere middle frontal gyrus, precentral gyrus, and frontal pole with greater age-related increases in FICVF in the ASD group compared to TD (Fig. 5). No significant age-by-group interactions were observed for ODI, FA, MD, RD, or AD. Neuroanatomical locations of significant age by group interactions on FICVF can be found in **Supplement** Table 2**.**

6.4. Associations with ADOS-2 CSS

Significant relationships between CSS and cortical microstructure (accounting for the effects of age and IQ) were observed with GBSS measures of ODI, MD, RD, and AD across widespread cortical regions within the ASD cohort ($p < 0.05$; FWER-corrected) (Fig. 6; **Supplement Table 3**). Negative relationships were observed between CSS and ODI, whereas positive relationships with CSS were observed between measures of MD, RD, and AD. While cortical areas of significance are widespread, significant areas are largely localized to the right hemisphere, complementary to our group difference findings.

When not accounting for the effects of IQ, Significant relationships ($p < 0.05$; FWER-corrected) were observed between CSS and cortical microstructure with GBSS measures of ODI, FA, MD, RD, and AD (**Supplement** Fig. 1**).** Findings follow the same directional relationships as observed when controlling for IQ. Additionally, FA was positively related to CSS.

6.5. Associations with SRS

Relationships between SRS and cortical microstructure were observed with GBSS measures (accounting for the effects of age and IQ); however, these relationships did not survive correction for multiple comparisons. SRS correlated positively with ODI, AD, and negatively with FICVF (uncorrected; $p < 0.01$) See **Supplement** Fig. 2 and **Supplement Table 4** for general brain areas where this relationship exists. Findings remain non-significant when not accounting for the effects of IQ in the linear model.

7. Discussion

The cortical microstructure is foundational for the brain's neural circuitry and is implicated in the developmental neural basis of ASD. In this work, we examined group and age-related differences of the cortical microstructure between autistic and TD males from childhood into young adulthood. We also sought to investigate relationships between cortical microstructure and measures of autistic symptoms. We report right-hemisphere differences in neurite density (FICVF) between autistic and TD males, as well as age-related differences between diagnostic groups. Specifically, we report decreased mean FICVF in the ASD group compared to TD, with a greater age-related increase in FICVF in ASD compared to TD, in non-overlapping voxels of the right hemisphere. It has been widely reported that the developmental trajectory of brain growth in autistic individuals follows an abnormally accelerated rate of early growth, followed by attenuated growth in childhood (Hazlett et al., 2005; Courchesne et al., 2001; Courchesne et al., 2003; Courchesne et al., 2011; Nordahl et al., 2011). This work supports our current findings of greater age-related increases in neurite density in ASD within the expected age-ranges of overgrowth, however, more work is needed to delineate microstructural age-related trajectories of gray matter that cannot be captured with volume-based analyses. We extend recent work utilizing multi-shell dMRI in ASD and use the GBSS framework (Nazeri et al., 2017) to assess cortical GM differences related to ASD. Our findings provide new insights into group and age-related differences of cortical GM microstructure in ASD, with implications for the role of cortical organization in the level of autistic symptoms and highlight NODDI as an important tool for delineating fine microstructural features of the cortex.

Consistent with our findings, a recent study reported a trend-level group difference of lower FICVF in the ASD group in areas of the cingulate gyrus, right superior temporal lobe and much of the parietal lobes (Carper et al., 2016). Differences in minicolumar cortical organization have also been reported in post-mortem studies of ASD (Casanova et al., 2002), described by narrower cells (Buxhoeveden et al., 2006) and reduced cell density in frontal brain regions (Casanova et al., 2006). Reductions in FICVF in autistic individuals may be related to thinning of myelinated axons in cortical GM (Groen et al., 2011), with age-by-group interactions of FICVF suggesting differential developmental timing of cortical thinning between groups. Indeed, age related differences in cortical thickness have been reported in autistic individuals 6-to-30 years (Nunes et al., 2020), with studies reporting thinner cortices during

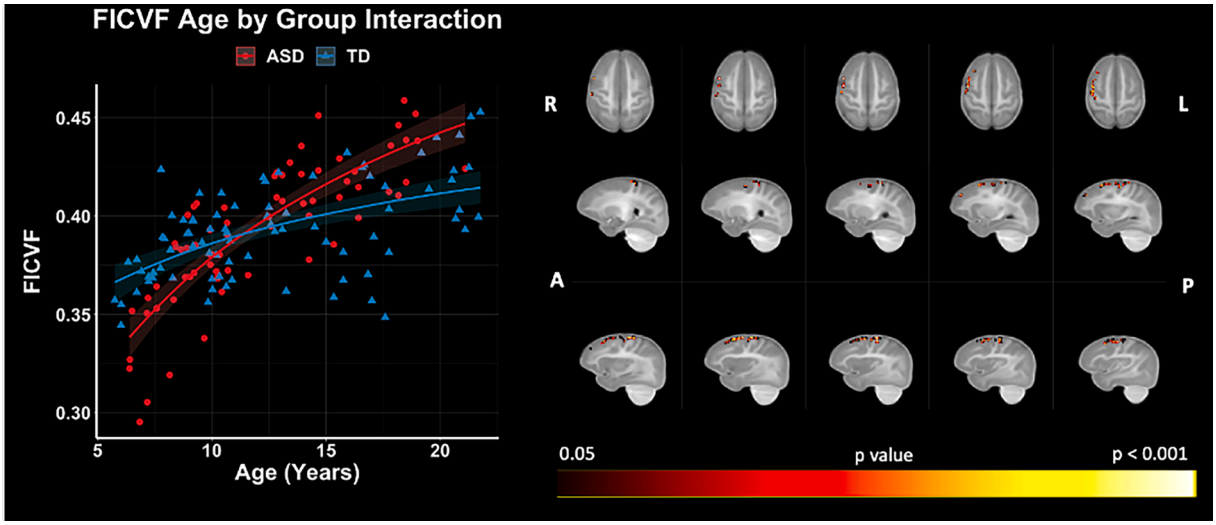

Fig. 5. NODDI FICVF age by group interactions. Level of significance and neuroanatomical location of voxels from interaction model are displayed on the mean FICVF map across all participants. Scatter plots represent mean FICVF values of significant voxels from each individual. Trendlines show model fit and confidence intervals for age by group interaction on dMRI measures when accounting for the effects of age and group.

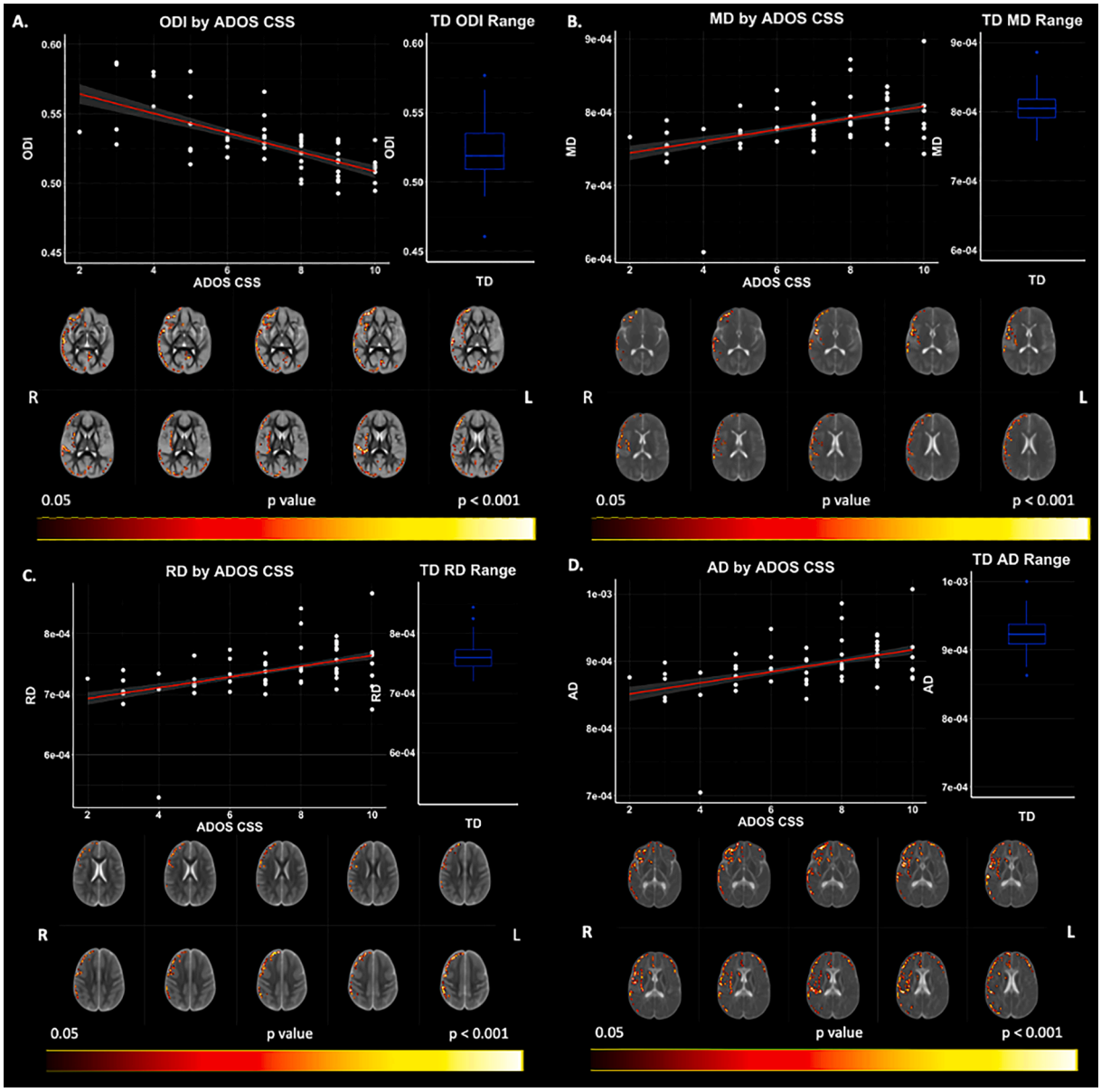

Fig. 6. ADOS-2 CSS by DWI Relationships in ASD Accounting for IQ as a Covariate. Level of significance and neuroanatomical location of significant voxels are displayed on the dMRI maps. Scatter plots represent mean dMRI values of significant voxels for each measure. Trendlines show model fit and confidence intervals for relationship between dMRI measures and ADOS CSS when accounting for the effects of age and IQ. Boxplots show TD range for DWI measures averaged over significant voxels.

childhood followed by increased cortical thickness during adulthood in subjects with ASD (Ecker et al., 2014).

GM microstructural group differences were observed to be concentrated to the right hemisphere in ASD, suggesting potential hemispheric-specific cortical differences in ASD (Floris et al., 2021; Postema et al., 2019) particularly within cognitive, social/emotional, sensory, and visual brain areas (Figs. 4-5; **Supplement** Table 1-2). Hemispheric specialization results from changes in cortical organization and supports specific functional processes such as analysis of auditory and language information in the left hemisphere (Hutsler and Galuske, 2003; Josse and Tzourio-Mazoyer, 2004), and downstream visual processing in the right hemisphere (Brederoo et al., 2020). While hemispheric asymmetry was not explicitly tested; the current work contributes to a growing body of evidence suggesting potential disruption of hemispheric specialization in ASD in both structural and functional organization of the cortex (Floris et al., 2021; Floris and Howells, 2018; Lindell and Hudry, 2013; Nielsen et al., 2014).

GM microstructure (ODI, MD, RD, AD) was also significantly related to the CSS in cortical brain areas (**Supplement Table 3**). We report higher CSS scores to be associated with lower ODI, and higher MD, RD, and AD. Across these measures, the frontal pole and the middle frontal gyrus were common regions of significance. While GM microstructure was not significantly associated with SRS, we found negative relationships between SRS and FICVF, and positive relationships with SRS and ODI and AD. Though SRS findings did not survive multiple comparison correction, together, these relationships suggest the level of autistic symptoms in ASD may be linked to altered GM microstructure. Interestingly, across dMRI measures, FICVF in the temporal fusiform cortex, an area largely responsible for facial and object recognition (Palejwala et al., 2020), is the only common brain region found to show the relationships between both GM microstructure and SRS and CSS scores, suggesting a more pervasive role of the structural architecture and organization of the temporal fusiform cortex in behavioral challenges related to ASD.

Our findings support the growing literature of differential cortical development in ASD in language (Joseph et al., 2014) and visual networks responsible for facial and object recognition and processing (Sato et al., 2017) and may provide additional evidence for sources of social challenges associated with ASD. Our findings also implicate GM microstructure of motor (precentral gyrus) (Banker and Neuroanatomy, 2021 2021.) and sensorimotor (frontal medial cortex) (Silva Moreira et al., 2016) functions, setting the stage for future studies to further examine the microstructural correlates of motor challenges related to ASD. Moreover, while not a core diagnostic trait of ASD, difficulties with executive functioning are common amongst autistic individuals (Lai et al., 2017). Here, we report age-related cortical microstructural differences of FICVF in GM of autistic individuals within the neural circuits of executive functioning, particularly within the right hemisphere frontal pole and middle frontal gyri, which contribute to cognitive and executive functions (Japee et al., 2015) ; for a review see (Hill, 2004). More work utilizing longitudinal multimodal assessment is needed to evaluate structure–function relationships in ASD particularly pertaining to GM processing centers.

Our study is limited by its cross-sectional design, all male participant samples, and the limitations of composite clinical measures of autistic symptom severity. Longitudinal study of age-related cortical microstructural changes within autistic individuals and TD are needed to support our findings of group and age-related developmental differences. Additional studies in autistic females and more cognitively-impaired individuals are additionally needed to expand the generalizability of our results. Furthermore, associations of cortical microstructural differences with CSS and SRS scores within the ASD sample provide convergent evidence that observed ASD-TDC cortical differences may be related to ASD rather than other potential (unmeasured) differences between the diagnostic groups. The ADOS-2 CSS and SRS scores have complementary strengths and limitations (Hus et al., 2013a,b, 2014; Gotham et al., 2007). The ADOS-2 is an investigator-based assessment of autistic symptoms observed during standardized interactional assessment at the time of evaluation. The SRS is a parent-based questionnaire focusing on a broader range of behaviors observed across a broader context and time frame. As the use of both clinical measures provides complementary information and is, therefore, a strength of this study, the set of autistic behaviors underlying an individual's CSS and SRS scores varies from individual to individual. As such, larger samples are needed to test more specific cortical microstructure-autistic behavior correlations, and longitudinal studies are needed to provide temporal insight into the emergence of these differential developmental trajectories.

Overall, the current study investigated GM microstructural differences in the cerebral cortex between autistic and TD individuals using dMRI and GBSS. Findings revealed group and age-related group differences in cortical GM organization in cortical brain areas involved in various cognitive, sensory, and motor functions. Furthermore, this study begins to bridge a critical gap knowledge of cortical brain organization related to ASD. To our knowledge, this study is the first to utilize NODDI and the GBSS framework to assess cortical GM microstructural differences in ASD and supports the hypothesis that alterations to the underlying cortical microstructure play an important role in ASD. Future studies are necessary to assess potential specific behavioral correlates of these atypical GM microstructure findings, while future longitudinal studies will be informative for assessing individual variation and investigating developmental changes over time.

CRediT authorship contribution statement

Marissa A. DiPiero: Conceptualization, Methodology, Software, Formal analysis, Investigation, Writing – original draft, Writing – review & editing, Visualization, Project administration. **Olivia J. Surgent:** Data curation, Investigation, Writing – review & editing, Visualization. **Brittany G. Travers:** Methodology, Resources, Data curation, Writing – review & editing, Supervision, Funding acquisition. **Andrew L. Alexander:** Conceptualization, Methodology, Resources, Data curation, Writing – review & editing, Supervision, Funding acquisition, Project administration. **Janet E. Lainhart:** Methodology, Resources, Data curation, Writing – review & editing, Supervision, Funding acquisition. **Douglas C. Dean III:** Conceptualization, Methodology, Software, Resources, Data curation, Resources, Writing – review & editing, Supervision, Funding acquisition, Project administration.

Declaration of Competing Interest

The authors declare that they have no known competing financial interests or personal relationships that could have appeared to influence the work reported in this paper.

Data availability

Data will be made available on request.

Acknowledgements

We sincerely thank our research participants and their families who participated in this research as well as the dedicated research staff who made this work possible. This work was supported by grants R01 MH097464 (Dr. Lainhart), R01 MH080826 (Dr. Lainhart), and R00 MH11056 (Dr. Dean) from the National Institute of Mental Health, National Institutes of Health. Infrastructure support was also provided, in part, by grant P50HD105353 from the Eunice Kennedy Shriver NICHD, National Institutes of Health (Waisman Center) and the Hartwell Foundation's Individual Biomedical Award (Dr. Travers). Authors, Marissa DiPiero and Olivia Surgent were also supported in part by NIH/NINDS T32 NS105602. The content is solely the responsibility of the authors and does not necessarily represent the official views of the National Institutes of Health.

Appendix A. Supplementary data

Supplementary data to this article can be found online at https://doi.org/10.1016/j.nicl.2022.103306.

References

Afzali, M., Pieciak, T., Newman, S., Garyfallidis, E., Ozarslan, E., Cheng, H., et al., 2021. The sensitivity of diffusion MRI to microstructural properties and experimental factors. J. Neurosci. Methods 347, 108951.
Alexander, D.C., Dyrby, T.B., Nilsson, M., Zhang, H., 2019. Imaging brain microstructure with diffusion MRI: practicality and applications. NMR Biomed. 32 (4), e3841.
Alexander, A.L., Hasan, K.M., Lazar, M., Tsuruda, J.S., Parker, D.L., 2001. Analysis of partial volume effects in diffusion-tensor MRI. Magn. Reson. Med. 45 (5), 770–780.
Amaral, D.G., Schumann, C.M., Nordahl, C.W., 2008. Neuroanatomy of autism. Trends Neurosci. 31 (3), 137–145.
Ameis, S.H., Catani, M., 2015. Altered white matter connectivity as a neural substrate for social impairment in Autism Spectrum Disorder. Cortex 62, 158–181.
Andersson, J.L.R., Graham, M.S., Zsoldos, E., Sotiropoulos, S.N., 2016. Incorporating outlier detection and replacement into a non-parametric framework for movement and distortion correction of diffusion MR images. Neuroimage 141, 556–572.
Andersson, J.L.R., Sotiropoulos, S.N., 2016. An integrated approach to correction for off-resonance effects and subject movement in diffusion MR imaging. Neuroimage 125, 1063–1078.
Association, A.P., American Psychiatric, A., American, P.A., 2013. Diagnostic and statistical manual of mental disorders : DSM-5, fifth ed. American Psychiatric Association, Arlington, VA.
Avants, B.B., Epstein, C.L., Grossman, M., Gee, J.C., 2008. Symmetric diffeomorphic image registration with cross-correlation: evaluating automated labeling of elderly and neurodegenerative brain. Med. Image Anal. 12 (1), 26–41.
Avants, B.B., Yushkevich, P., Pluta, J., Minkoff, D., Korczykowski, M., Detre, J., et al., 2010. The optimal template effect in hippocampus studies of diseased populations. Neuroimage 49 (3), 2457–2466.
Avants, B.B., Tustison, N.J., Wu, J., Cook, P.A., Gee, J.C., 2011. An open source multivariate framework for n-tissue segmentation with evaluation on public data. Neuroinformatics 9 (4), 381–400.
Banker, L., Neuroanatomy, T.P., 2021 2021.. Precentral Gyrus. StatPearls Publishing, Treasure Island (FL).

Basser, P.J., 1995. Inferring microstructural features and the physiological state of tissues from diffusion-weighted images. NMR Biomed. 8 (7–8), 333–344.
Basser, P.J., Ozarslan, E., 2009. Introduction to Diffusion MR. From Quantitative Measurement to in Vivo Neuroanatomy, Diffusion Mri, pp. 3–10.
Bedford, S.A., Park, M.T.M., Devenyi, G.A., Tullo, S., Germann, J., Patel, R., et al., 2020. Large-scale analyses of the relationship between sex, age and intelligence quotient heterogeneity and cortical morphometry in autism spectrum disorder. Mol. Psychiatry 25 (3), 614–628.
Bletsch, A., Schafer, T., Mann, C., Andrews, D.S., Daly, E., Gudbrandsen, M., et al., 2021. Atypical measures of diffusion at the gray-white matter boundary in autism spectrum disorder in adulthood. Hum. Brain Mapp. 42 (2), 467–484.
Brederoo, S.G., Van der Haegen, L., Brysbaert, M., Nieuwenstein, M.R., Cornelissen, F.W., Lorist, M.M., 2020. Towards a unified understanding of lateralized vision: A large-scale study investigating principles governing patterns of lateralization using a heterogeneous sample. Cortex 133, 201–214.
Buxhoeveden, D.P., Semendeferi, K., Buckwalter, J., Schenker, N., Switzer, R., Courchesne, E., 2006. Reduced minicolumns in the frontal cortex of patients with autism. Neuropathol. Appl. Neurobiol. 32 (5), 483–491.
Carper, R.A., Treiber, J.M., White, N.S., Kohli, J.S., Muller, R.A., 2016. Restriction Spectrum Imaging As a Potential Measure of Cortical Neurite Density in Autism. Front. Neurosci. 10, 610.
Casanova, M.F., Buxhoeveden, D.P., Brown, C., 2002. Clinical and Macroscopic Correlates of Minicolumnar Pathology in Autism. J. Child Neurol. 17 (9), 692–695.
Casanova, M.F., van Kooten, I.A., Switala, A.E., van Engeland, H., Heinsen, H., Steinbusch, H.W., et al., 2006. Minicolumnar abnormalities in autism. Acta Neuropathol. 112 (3), 287–303.
Constantino, J.N., Gruber, C.P., 2012. Social responsiveness scale: SRS-2: Western psychological services Torrance. CA.
Courchesne, E., Karns, C.M., Davis, H.R., Ziccardi, R., Carper, R.A., Tigue, Z.D., et al., 2001. Unusual brain growth patterns in early life in patients with autistic disorder: an MRI study. Neurology 57 (2), 245–254.
Courchesne, E., Carper, R., Akshoomoff, N., 2003. Evidence of brain overgrowth in the first year of life in autism. J. Am. Med. Assoc. 290 (3), 337–344.
Courchesne, E., Mouton, P.R., Calhoun, M.E., Semendeferi, K., Ahrens-Barbeau, C., Hallet, M.J., et al., 2011. Neuron number and size in prefrontal cortex of children with autism. J. Am. Med. Assoc. 306 (18), 2001–2010.
Courchesne, E., Campbell, K., Solso, S., 2011. Brain growth across the life span in autism: age-specific changes in anatomical pathology. Brain Res. 1380, 138–145.
Wechsler Da. WASI-II : Wechsler abbreviated scale of intelligence: Second edition. Bloomington, MN : PsychCorp, [2011] ©2011; 2011.
Daducci, A., Canales-Rodriguez, E.J., Zhang, H., Dyrby, T.B., Alexander, D.C., Thiran, J. P., 2015. Accelerated Microstructure Imaging via Convex Optimization (AMICO) from diffusion MRI data. Neuroimage 105, 32–44.
Dean 3rd, D.C., Travers, B.G., Adluru, N., Tromp do, P.M., Destiche, D.J., Samsin, D., et al., 2016. Investigating the microstructural correlation of white matter in autism spectrum disorder. Brain Connect 6 (5), 415–433.
Desikan, R.S., Ségonne, F., Fischl, B., Quinn, B.T., Dickerson, B.C., Blacker, D., et al., 2006. An automated labeling system for subdividing the human cerebral cortex on MRI scans into gyral based regions of interest. Neuroimage 31 (3), 968–980.
Ecker, C., Ginestet, C., Feng, Y., Johnston, P., Lombardo, M.V., Lai, M.C., et al., 2013. Brain surface anatomy in adults with autism: the relationship between surface area, cortical thickness, and autistic symptoms. JAMA Psychiat. 70 (1), 59–70.
Ecker, C., Shahidiani, A., Feng, Y., Daly, E., Murphy, C., D'Almeida, V., et al., 2014. The effect of age, diagnosis, and their interaction on vertex-based measures of cortical thickness and surface area in autism spectrum disorder. J. Neural Transm. (Vienna) 121 (9), 1157–1170.
Edgar, J.C., Dipiero, M., McBride, E., Green, H.L., Berman, J., Ku, M., et al., 2019. Abnormal maturation of the resting-state peak alpha frequency in children with autism spectrum disorder. Hum. Brain Mapp. 40 (11), 3288–3298.
Fan, L., Jiang, T., 2017. Mapping underlying maturational changes in human brain. Neurosci. Bull. 33 (4), 478–480.
Floris, D.L., Howells, H., 2018. Atypical structural and functional motor networks in autism. Prog. Brain Res. 238, 207–248.
Floris, D.L., Wolfers, T., Zabihi, M., Holz, N.E., Zwiers, M.P., Charman, T., et al., 2021. Atypical brain asymmetry in autism-A candidate for clinically meaningful stratification. Biol Psychiatry Cogn Neurosci Neuroimaging. 6 (8), 802–812.
Fortin, J.-P., Cullen, N., Sheline, Y.I., Taylor, W.D., Aselcioglu, I., Cook, P.A., et al., 2018. Harmonization of cortical thickness measurements across scanners and sites. Neuroimage 167, 104–120.
Frazier, J.A., Chiu, S., Breeze, J.L., Makris, N., Lange, N., Kennedy, D.N., et al., 2005. Structural brain magnetic resonance imaging of limbic and thalamic volumes in pediatric bipolar disorder. Am. J. Psychiatry 162 (7), 1256–1265.
Garyfallidis, E., Brett, M., Amirbekian, B., Rokem, A., van der Walt, S., Descoteaux, M., et al., 2014. Dipy, a library for the analysis of diffusion MRI data. Front. Neuroinf. 8, 8.
Gogtay, N., Giedd, J.N., Lusk, L., Hayashi, K.M., Greenstein, D., Vaituzis, A.C., et al., 2004. Dynamic mapping of human cortical development during childhood through early adulthood. PNAS 101 (21), 8174–8179.
Goldstein, J.M., Seidman, L.J., Makris, N., Ahern, T., O'Brien, L.M., Caviness Jr, V.S., et al., 2007. Hypothalamic abnormalities in schizophrenia: sex effects and genetic vulnerability. Biol. Psychiatry 61 (8), 935–945.
Gotham, K., Risi, S., Pickles, A., Lord, C., 2007. The Autism Diagnostic Observation Schedule: revised algorithms for improved diagnostic validity. J. Autism Dev. Disord. 37 (4), 613–627.
Gotham, K., Pickles, A., Lord, C., 2009. Standardizing ADOS scores for a measure of severity in autism spectrum disorders. J. Autism Dev. Disord. 39 (5), 693–705.
Green, H.L., Dipiero, M., Koppers, S., Berman, J.I., Bloy, L., Liu, S., et al., 2022. Peak alpha frequency and thalamic structure in children with typical development and autism spectrum disorder. J. Autism Dev. Disord. 52 (1), 103–112.
Groen, W.B., Buitelaar, J.K., van der Gaag, R.J., Zwiers, M.P., 2011. Pervasive microstructural abnormalities in autism: a DTI study. J. Psychiatry Neurosci. 36 (1), 32–40.
Hardan, A.Y., Jou, R.J., Keshavan, M.S., Varma, R., Minshew, N.J., 2004. Increased frontal cortical folding in autism: a preliminary MRI study. Psychiatry Res. 131 (3), 263–268.
Hardan, A.Y., Libove, R.A., Keshavan, M.S., Melhem, N.M., Minshew, N.J., 2009. A preliminary longitudinal magnetic resonance imaging study of brain volume and cortical thickness in autism. Biol. Psychiatry 66 (4), 320–326.
Hazlett, H.C., Poe, M., Gerig, G., Smith, R.G., Provenzale, J., Ross, A., et al., 2005. Magnetic resonance imaging and head circumference study of brain size in autism: birth through age 2 years. Arch. Gen. Psychiatry 62 (12), 1366–1376.
Hazlett, H.C., Poe, M.D., Gerig, G., Styner, M., Chappell, C., Smith, R.G., et al., 2011. Early brain overgrowth in autism associated with an increase in cortical surface area before age 2 years. Arch. Gen. Psychiatry 68 (5), 467–476.
Hill, E.L., 2004. Executive dysfunction in autism. Trends Cogn. Sci. 8 (1), 26–32.
Hus, V., Bishop, S., Gotham, K., Huerta, M., Lord, C., 2013. Factors influencing scores on the social responsiveness scale. J Child Psychol. Psychiatry 54 (2), 216–224.
Hus, V., Bishop, S., Gotham, K., Huerta, M., Lord, C., 2013. Commentary: Advancing measurement of ASD severity and social competence: a reply to Constantino and Frazier (2013). J Child Psychol. Psychiatry 54 (6), 698–700.
Hus, V., Gotham, K., Lord, C., 2014. Standardizing ADOS domain scores: separating severity of social affect and restricted and repetitive behaviors. J. Autism Dev. Disord. 44 (10), 2400–2412.
Hus, V., Lord, C., 2014. The autism diagnostic observation schedule, module 4: revised algorithm and standardized severity scores. J. Autism Dev. Disord. 44 (8), 1996–2012.
Hutsler, J., Galuske, R.A., 2003. Hemispheric asymmetries in cerebral cortical networks. Trends Neurosci. 26 (8), 429–435.
James III, P., 1975. Statistical Inference Using Extreme Order Statistics. The Annals of Statistics 3 (1), 119–131.
Japee, S., Holiday, K., Satyshur, M.D., Mukai, I., Ungerleider, L.G., 2015. A role of right middle frontal gyrus in reorienting of attention: a case study. Front. Syst. Neurosci. 9, 23.
Jenkinson, M., Bannister, P., Brady, M., Smith, S., 2002. Improved optimization for the robust and accurate linear registration and motion correction of brain images. Neuroimage 17, 825–841.
Jenkinson, M., Beckmann, C.F., Behrens, T.E., Woolrich, M.W., Smith, S.M., 2012. Fsl. Neuroimage. 62 (2), 782–790.
Joseph, R.M., Fricker, Z., Fenoglio, A., Lindgren, K.A., Knaus, T.A., Tager-Flusberg, H., 2014. Structural asymmetries of language-related gray and white matter and their relationship to language function in young children with ASD. Brain Imaging Behav. 8 (1), 60–72.
Josse, G., Tzourio-Mazoyer, N., 2004. Hemispheric specialization for language. Brain Res. Brain Res. Rev. 44 (1), 1–12.
Kellner, E., Dhital, B., Kiselev, V.G., Reisert, M., 2016. Gibbs-ringing artifact removal based on local subvoxel-shifts. Magn. Reson. Med. 76 (5), 1574–1581.
Khundrakpam, B.S., Lewis, J.D., Kostopoulos, P., Carbonell, F., Evans, A.C., 2017. Cortical thickness abnormalities in autism spectrum disorders through late childhood, adolescence, and adulthood: a large-scale MRI study. Cereb. Cortex 27 (3), 1721–1731.
Kohli, J.S., Kinnear, M.K., Fong, C.H., Fishman, I., Carper, R.A., Muller, R.A., 2019. Local cortical gyrification is increased in children with autism spectrum disorders, but decreases rapidly in adolescents. Cereb. Cortex 29 (6), 2412–2423.
Lai, C.L.E., Lau, Z., Lui, S.S.Y., Lok, E., Tam, V., Chan, Q., et al., 2017. Meta-analysis of neuropsychological measures of executive functioning in children and adolescents with high-functioning autism spectrum disorder. Autism Res. 10 (5), 911–939.
Lainhart, J.E., 2015. Brain imaging research in autism spectrum disorders: in search of neuropathology and health across the lifespan. Curr. Opin. Psychiatry 28 (2), 76–82.
Lange, N., Travers, B.G., Bigler, E.D., Prigge, M.B., Froehlich, A.L., Nielsen, J.A., et al., 2015. Longitudinal volumetric brain changes in autism spectrum disorder ages 6–35 years. Autism Res. 8 (1), 82–93.
Lebel, C., Walker, L., Leemans, A., Phillips, L., Beaulieu, C., 2008. Microstructural maturation of the human brain from childhood to adulthood. Neuroimage 40 (3), 1044–1055.
Leemans, A., Jones, D.K., 2009. The B-matrix must be rotated when correcting for subject motion in DTI data. Magn. Reson. Med. 61 (6), 1336–1349.
Lindell, A.K., Hudry, K., 2013. Atypicalities in cortical structure, handedness, and functional lateralization for language in autism spectrum disorders. Neuropsychol. Rev. 23 (3), 257–270.
Lord, C., Risi, S., Lambrecht, L., Cook Jr., E.H., Leventhal, B.L., DiLavore, P.C., et al., 2000. The autism diagnostic observation schedule-generic: a standard measure of social and communication deficits associated with the spectrum of autism. J. Autism Dev. Disord. 30 (3), 205–223.
Makris, N., Goldstein, J.M., Kennedy, D., Hodge, S.M., Caviness, V.S., Faraone, S.V., et al., 2006. Decreased volume of left and total anterior insular lobule in schizophrenia. Schizophr. Res. 83 (2), 155–171.
Matsuoka, K., Makinodan, M., Kitamura, S., Takahashi, M., Yoshikawa, H., Yasuno, F., et al., 2020. Increased dendritic orientation dispersion in the left occipital gyrus is associated with atypical visual processing in adults with autism spectrum disorder. Cereb. Cortex 30 (11), 5617–5625.

McKenna, F., Miles, L., Donaldson, J., Castellanos, F.X., Lazar, M., 2020. Diffusion kurtosis imaging of gray matter in young adults with autism spectrum disorder. Sci. Rep. 10 (1), 21465.
Mensen, V.T., Wierenga, L.M., van Dijk, S., Rijks, Y., Oranje, B., Mandl, R.C., et al., 2017. Development of cortical thickness and surface area in autism spectrum disorder. Neuroimage Clin. 13, 215–222.
Minshew, N.J., Williams, D.L., 2007. The new neurobiology of autism: cortex, connectivity, and neuronal organization. Arch. Neurol. 64 (7), 945–950.
Nazeri, A., Chakravarty, M.M., Rotenberg, D.J., Rajji, T.K., Rathi, Y., Michailovich, O.V., et al., 2015. Functional consequences of neurite orientation dispersion and density in humans across the adult lifespan. J. Neurosci. 35 (4), 1753–1762.
Nazeri, A., Mulsant, B.H., Rajji, T.K., Levesque, M.L., Pipitone, J., Stefanik, L., et al., 2017. Gray Matter Neuritic Microstructure Deficits in Schizophrenia and Bipolar Disorder. Biol. Psychiatry 82 (10), 726–736.
Nielsen, J.A., Zielinski, B.A., Fletcher, P.T., Alexander, A.L., Lange, N., Bigler, E.D., et al., 2014. Abnormal lateralization of functional connectivity between language and default mode regions in autism. Mol Autism. 5 (1), 8.
Nordahl, C.W., Lange, N., Li, D.D., Barnett, L.A., Lee, A., Buonocore, M.H., et al., 2011. Brain enlargement is associated with regression in preschool-age boys with autism spectrum disorders. PNAS 108 (50), 20195–20200.
Nunes, A.S., Vakorin, V.A., Kozhemiako, N., Peatfield, N., Ribary, U., Doesburg, S.M., 2020. Atypical age-related changes in cortical thickness in autism spectrum disorder. Sci. Rep. 10 (1), 11067.
Ohta, H., Nordahl, C.W., Iosif, A.M., Lee, A., Rogers, S., Amaral, D.G., 2016. Increased Surface Area, but not Cortical Thickness, in a Subset of Young Boys With Autism Spectrum Disorder. Autism Res. 9 (2), 232–248.
Palejwala, A.H., O'Connor, K.P., Milton, C.K., Anderson, C., Pelargos, P., Briggs, R.G., et al., 2020. Anatomy and white matter connections of the fusiform gyrus. Sci. Rep. 10 (1), 13489.
Palmen, S.J., van Engeland, H., Hof, P.R., Schmitz, C., 2004. Neuropathological findings in autism. Brain 127 (Pt 12), 2572–2583.
Pichiecchio, A., Carigi, T., 2016. Brain Diffusion Tensor Imaging and Volumetric Analysis: Grey and White Matter Changes in Preschool Children with Autism Spectrum Disorder. Autism-Open. Access 06 (01).
Piven, J., Elison, J.T., Zylka, M.J., 2017. Toward a conceptual framework for early brain and behavior development in autism. Mol. Psychiatry 22 (10), 1385–1394.
Pomponio, R., Erus, G., Habes, M., Doshi, J., Srinivasan, D., Mamourian, E., et al., 2020. Harmonization of large MRI datasets for the analysis of brain imaging patterns throughout the lifespan. Neuroimage 208, 116450.
Postema, M.C., van Rooij, D., Anagnostou, E., Arango, C., Auzias, G., Behrmann, M., et al., 2019. Altered structural brain asymmetry in autism spectrum disorder in a study of 54 datasets. Nat. Commun. 10 (1), 4958.
Prigge, M.B.D., Bigler, E.D., Travers, B.G., Froehlich, A., Abildskov, T., Anderson, J.S., et al., 2018. Social responsiveness scale (SRS) in relation to longitudinal cortical thickness changes in autism spectrum disorder. J. Autism Dev. Disord. 48 (10), 3319–3329.
Prigge, M.B.D., Lange, N., Bigler, E.D., King, J.B., Dean 3rd, D.C., Adluru, N., et al., 2021. A 16-year study of longitudinal volumetric brain development in males with autism. Neuroimage 236, 118067.
R Core Team, 2021. R: A language and environment for statistical computing. R Foundation for Statistical Computing,, Vienna, Austria.
Sato, W., Kochiyama, T., Uono, S., Yoshimura, S., Kubota, Y., Sawada, R., et al., 2017. Reduced Gray Matter Volume in the Social Brain Network in Adults with Autism Spectrum Disorder. Front. Hum. Neurosci. 11, 395.
Silva Moreira, P., Marques, P., Magalhães, R., 2016. Identifying Functional Subdivisions in the Medial Frontal Cortex. J. Neurosci. 36 (44), 11168–11170.
Smith, S.M., 2002. Fast robust automated brain extraction. Hum. Brain Mapp. 17 (3), 143–155.
Smith, S.M., Jenkinson, M., Johansen-Berg, H., Rueckert, D., Nichols, T.E., Mackay, C.E., et al., 2006. Tract-based spatial statistics: voxelwise analysis of multi-subject diffusion data. Neuroimage 31 (4), 1487–1505.
Smith, S.M., Nichols, T.E., 2009. Threshold-free cluster enhancement: addressing problems of smoothing, threshold dependence and localisation in cluster inference. Neuroimage 44 (1), 83–98.
Smith, E., Thurm, A., Greenstein, D., Farmer, C., Swedo, S., Giedd, J., et al., 2016. Cortical thickness change in autism during early childhood. Hum. Brain Mapp. 37 (7), 2616–2629.
Surgent, O.J., Walczak, M., Zarzycki, O., Ausderau, K., Travers, B.G., 2021. IQ and Sensory Symptom Severity Best Predict Motor Ability in Children With and Without Autism Spectrum Disorder. J. Autism Dev. Disord. 51 (1), 243–254.
Tamnes, C.K., Ostby, Y., Fjell, A.M., Westlye, L.T., Due-Tonnessen, P., Walhovd, K.B., 2010. Brain maturation in adolescence and young adulthood: regional age-related changes in cortical thickness and white matter volume and microstructure. Cereb. Cortex 20 (3), 534–548.
Tournier, J.D., Smith, R., Raffelt, D., Tabbara, R., Dhollander, T., Pietsch, M., et al., 2019. MRtrix3: A fast, flexible and open software framework for medical image processing and visualisation. Neuroimage 202, 116137.
Travers, B.G., Tromp do, P.M., Adluru, N., Lange, N., Destiche, D., Ennis, C., et al., 2015. Atypical development of white matter microstructure of the corpus callosum in males with autism: a longitudinal investigation. Mol. Autism 6, 15.
Turesky, T.K., Vanderauwera, J., Gaab, N., 2021. Imaging the rapidly developing brain: Current challenges for MRI studies in the first five years of life. Dev. Cogn. Neurosci. 47, 100893.
Uono, S., Sato, W., Kochiyama, T., Yoshimura, S., Sawada, R., Kubota, Y., et al., 2022. The structural neural correlates of atypical facial expression recognition in autism spectrum disorder. Brain Imaging Behav.
Vargas, D.L., Nascimbene, C., Krishnan, C., Zimmerman, A.W., Pardo, C.A., 2005. Neuroglial activation and neuroinflammation in the brain of patients with autism. Ann. Neurol. 57 (1), 67–81.
Veraart, J., Novikov, D.S., Christiaens, D., Ades-Aron, B., Sijbers, J., Fieremans, E., 2016. Denoising of diffusion MRI using random matrix theory. Neuroimage 142, 394–406.
Wallace, G.L., Eisenberg, I.W., Robustelli, B., Dankner, N., Kenworthy, L., Giedd, J.N., et al., 2015. Longitudinal cortical development during adolescence and young adulthood in autism spectrum disorder: increased cortical thinning but comparable surface area changes. J. Am. Acad. Child Adolesc. Psychiatry 54 (6), 464–469.
Wheeler-Kingshott, C.A., Cercignani, M., 2009. About, "axial" and "radial" diffusivities. Magn. Reson. Med. 61 (5), 1255–1260.
Williams, E.L., El-Baz, A., Nitzken, M., Switala, A.E., Casanova, M.F., 2012. Spherical harmonic analysis of cortical complexity in autism and dyslexia. Transl. Neurosci. 3 (1), 36–40.
Winkler, A.M., Ridgway, G.R., Webster, M.A., Smith, S.M., Nichols, T.E., 2014. Permutation inference for the general linear model. Neuroimage 92, 381–397.
Winkler, A.M., Webster, M.A., Brooks, J.C., Tracey, I., Smith, S.M., Nichols, T.E., 2016. Non-parametric combination and related permutation tests for neuroimaging. Hum. Brain Mapp. 37, 1486–1511. https://doi.org/10.1002/hbm.23115.
Yang, D.Y., Beam, D., Pelphrey, K.A., Abdullahi, S., Jou, R.J., 2016. Cortical morphological markers in children with autism: a structural magnetic resonance imaging study of thickness, area, volume, and gyrification. Mol Autism. 7, 11.
Yasuno, F., Makinodan, M., Takahashi, M., Matsuoka, K., Yoshikawa, H., Kitamura, S., et al., 2020. Microstructural anomalies evaluated by neurite orientation dispersion and density imaging are related to deficits in facial emotional recognition via perceptual-binding difficulties in autism spectrum disorder. Autism Res. 13 (5), 729–740.
Zhang, H., Schneider, T., Wheeler-Kingshott, C.A., Alexander, D.C., 2012. NODDI: practical in vivo neurite orientation dispersion and density imaging of the human brain. Neuroimage 61 (4), 1000–1016.
Zielinski, B.A., Prigge, M.B., Nielsen, J.A., Froehlich, A.L., Abildskov, T.J., Anderson, J. S., et al., 2014. Longitudinal changes in cortical thickness in autism and typical development. Brain 137 (Pt 6), 1799–1812.